Role of cohesive energy in droplet fragmentation

Si Neng Sun and Herbert M. Urbassek*

Fachbereich Physik und Forschungszentrum für Optik und Materialwissenschaften OPTIMAS, Universität Kaiserslautern, Erwin-Schrödinger-Straße, D-67663 Kaiserslautern, Germany

(Received 28 August 2011; revised manuscript received 28 October 2011; published 18 November 2011)

Using molecular-dynamics simulation, we investigate the fragmentation behavior of droplets after collision with a wall. We demonstrate that the ratio of the impact to the cohesive energy E_{coh} of the droplet is the key quantity characterizing the droplet fragmentation process. To show this both van der Waals–bonded Ar and N_2 droplets and polar H_2O droplets are studied. If the impact energy per molecule $E < (0.35–0.4)E_{coh}$, the droplet is reflected without fragmenting. Beyond that impact energy fragmentation of the droplet abruptly starts. At $E = E_{coh}$, the fragmentation process already results in a fine dispersal of the droplet into daughter droplets; the maximum fragment contains only less than 4% of the initial droplet mass and around one-third of the droplet has been shattered into isolated molecules. The disintegration process continuously increases with collision energy. These findings are relevant for the process of droplet fragmentation as used in the method of impact desolvation of electrosprayed microdroplets mass spectrometry.

DOI: 10.1103/PhysRevE.84.056315 PACS number(s): 79.20.Ap, 82.80.Ms, 36.40.Qv, 34.35.+a

I. INTRODUCTION

Cluster- or droplet-wall collisions are of interest in a variety of situations ranging from controlled cluster deposition [1] over surface cleaning by cluster impact [2] to cluster-impact chemistry [3]. Recently such collisions have also found applications as a mass spectrometric technique: impact desolvation of electrosprayed microdroplets (IDEM) [4]. In this method the analyte molecule is solvated in a (highly charged) microdroplet prepared by an electrospray process; the droplet is accelerated through a potential difference and collided with a wall with the aim of desolvating the analyte without destroying it. While the IDEM method is but one of several competing techniques used for the mass spectrometry of macromolecules, our paper focuses on the physical mechanism underlying it, viz., the droplet fragmentation process.

The question arises as to what the optimum impact energy is; the answer will depend on the properties of the analyte molecule and on the analyte-droplet interaction. However, the energy also depends on the properties of the solvent, usually water or methanol. In this paper we focus on the latter aspect and consider pure droplets, i.e., without the inclusion of a solvated macromolecule; an extension to analyte-filled droplets is beyond the scope of the present work [5]. We shall demonstrate here that it is mainly one property of the solvent, its cohesive energy E_{coh}, that determines the fragmentation behavior of the droplet; this renders its fragmentation behavior universal once the impact energy has been scaled to E_{coh}. Certainly, the analyte-droplet interaction is decisive in determining whether and when the analyte is completely desolvated; this dependence, however, is not universal and will be analyzed elsewhere [5]. We note that droplet fragmentation patterns have been studied previously for clusters composed of van der Waals–bonded atoms [6–9] and molecules [10,11] and also for water [12,13], but in the present work we analyze the role of the cohesive energy.

Many aspects of droplet- and cluster-wall collisions have been studied theoretically over the years. Macroscopic impacts are covered by the method of fluid dynamics; see Ref. [14] for a recent study. A recent review [15] assembles the available knowledge on droplet intact reflection (called bouncing) and fragmentation (subdivided into splashing, spreading, and fingering).

The central message of our paper is that the ratio of the impact to the cohesive energy E_{coh} of the droplet is the key quantity characterizing the droplet fragmentation process. This applies to both the temporal dynamics and the size distribution of fragments as characterized by the quantities reported in Table I below. We show that droplet fragmentation starts at impact energies considerably below $E = E_{coh}$, namely, around $(0.35–0.4)E_{coh}$, while at $E = E_{coh}$ the fragmentation process already results in a fine dispersal of the droplet into daughter droplets.

II. METHOD

We study the fragmentation behavior of droplets of three widely differing materials after impact on a repulsive wall: Ar, as an example of a simple, van der Waals–bonded material; N_2, as a molecular material with similar bonding characteristics and whose fragmentation characteristics are well studied [10,11]; and water. The interaction potential in Ar [16] as well as in N_2 [11,17,18] is of a Lennard-Jones form; the weak quadrupole interaction present in the latter material is neglected. Water interacts with the TIP4P potential [19]; note that molecular vibration cannot be excited in this potential. We keep also the N_2 molecules rigid since the high vibrational quantum will not allow vibrational excitation at the collision energies studied here. The cohesive energy amounts to $E_{coh} = 80$, 75, and 520 meV in Ar, N_2, and H_2O [20]. We note that in our droplets, the average potential energy per molecule is smaller than these values due to the influence of the droplet surface, as well as the nonvanishing temperature, and amounts to 68, 65, and 438 meV, respectively.

The wall is modeled to be hard, i.e., its cohesive energy is assumed to be far above that of the droplet, and purely

*urbassek@rhrk.uni-kl.de; http://www.physik.uni-kl.de/urbassek/

TABLE I. Thresholds of scaled energies E/E_{coh}, beyond which fragmentation sets in or becomes dominant.

Droplet	$N_{\mathrm{fr}}/n > 10\%$	$\langle m\rangle/n < 10\%$	$m_{\mathrm{max}}/n < 10\%$	$N_{\mathrm{mono}}/n > 50\%$
Ar	0.35	0.29	0.66	3.80
N_2	0.40	0.40	0.72	1.50
H_2O	0.38	0.36	0.63	1.72

repulsive. This appears to be a good approximation for the impact of condensed-gas clusters on metal walls and even for water clusters at not too high velocities. Our neglect of any adhesion between the cluster and the wall appears justified for the condensed-gas clusters at not too small speeds and restricts our analysis to hydrophobic surfaces in the case of water impacts. The effect of the wall on the droplet molecules is modeled by a purely repulsive rigid external potential [10,11], which acts on each cluster atom.

The molecular-dynamics code is standard [11,21]. It employs the velocity Verlet integrator to solve Newton's equations of motion with a time step of 1 fs. The cluster is initially positioned at a distance in front of the wall such that the cluster has no interaction with it. The simulation is then started by giving each atom the same velocity toward the surface.

We present results for droplets containing $n = 9000$ molecules; simulations with smaller droplet sizes ($n \geqslant 3000$) gave almost identical result. We note, however, that the droplets investigated here have diameters of around 8 nm and thus are smaller than in typical experiments; for instance, in the IDEM method droplets possess diameters of around 100 nm [4]. Systematic investigation of such large clusters by atomistic simulation appears hardly possible due to the excessively large computation times. Our droplets have a finite temperature of $T = 40$ K (amorphous Ar and N_2) and 300 K (liquid water) in order to be closer to experiment. The total energy per molecule when impacting on the wall is hence $E = E_{\mathrm{imp}} + E_{\mathrm{th}}$, where E_{imp} is the kinetic center-of-mass energy of the droplet and E_{th} is the thermal energy per molecule at the initial temperature. We checked that a change in the initial cluster temperature T (for constant E) does not affect the fragmentation patterns discussed below. In particular, we observed no difference between the fragmentation of cold amorphous and warmer liquid droplets.

The simulations lasted 300 ps and were repeated three times with different impact conditions (droplet orientations) in order to gather statistics. The droplets impact with an energy per molecule E [varied in the range of $(0.2–3.8)E_{\mathrm{coh}}$] on the wall. The velocity of a droplet moving with $E = E_{\mathrm{coh}}$ amounts to 0.60, 0.68, and 2.18 km/s for Ar, N_2, and H_2O, respectively. Only perpendicular impacts are studied.

III. RESULTS

In Fig. 1 we exemplify the result of the collision of the $(H_2O)_{9000}$ droplet with the wall. Three collision energies have been chosen, which demonstrate different fragmentation regimes: the regime of (almost) intact reflection [Fig. 1(a)], in which only 30 water molecules were shed off the droplet; and the fragmentation regime [Figs. 1(b) and 1(c)], which shows increasing destruction of the droplet with increasing energy. In a sense to be quantified below (see Table I and its discussion), Fig. 1(b) belongs to the onset of fragmentation, while Fig. 1(c) shows fully developed fragmentation. The regime of complete disintegration or atomization is not reached at the energies studied here; previous studies [10] showed that the impact energy must be of the order of $E = 100E_{\mathrm{coh}}$ in order to destroy all intermolecular bonds.

The time evolution of N_2 droplet fragmentation is shown in Fig. 2; we note that the fragmentation dynamics of Ar and H_2O droplets have similar behavior and a comparison will be given below (see Fig. 3). The collision and fragmentation process can be divided into four stages: (i) During the compression stage, 0–5 ps, the translational kinetic energy E is transferred into internal energy (heat and pressure) of the cluster.

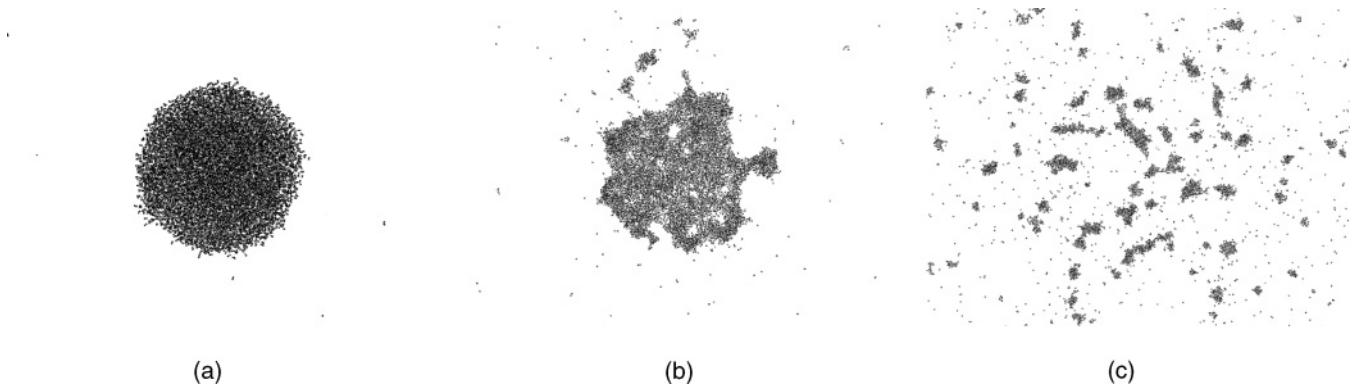

FIG. 1. Snapshots of the fragmentation of a $(H_2O)_{9000}$ droplet with impact energy per molecule of $E/E_{\mathrm{coh}} = 0.23$ (a), 0.51 (b), and 1.03 (c). The snapshots are taken at 25 ps and represent the regimes of (a) intact reflection, (b) onset of fragmentation, and (c) fully developed fragmentation. (b) and (c) show the fragmented droplet from a farther distance than (a) in order to include a larger part of the fragments created.

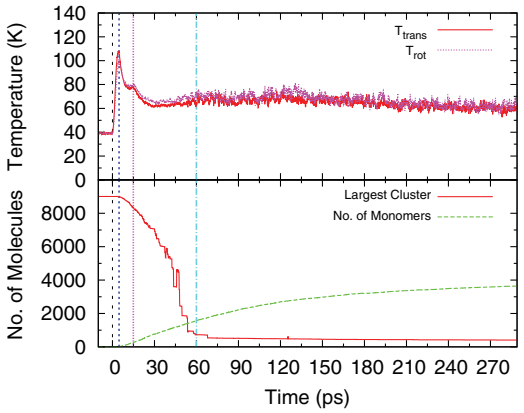

FIG. 2. (Color online) Fragmentation dynamics of a N_2 droplet with $E/E_{coh} = 1.00$. The top shows the evolution of the translational T_{trans} and rotational T_{rot} temperatures. The bottom shows the evolution of the number of molecules in the largest cluster m_{max} and of the number of free monomers N_{mono}. The droplet collides with the wall at the dashed line ($t = 0$). The other vertical lines divide the fragmentation process into four stages: compression, lateral jetting, void formation, and evaporation.

(ii) From 5 to 14 ps, the compressive pressure induces cluster reexpansion. This expansion occurs mainly sideways, i.e., along the wall, while the remainder of the cluster still continues moving toward the wall. Accordingly, this stage has been termed lateral expansion or lateral jetting [11,22,23]. Due to (adiabatic) expansion, thermal energy of the molecules is transferred to intermolecular potential energy; therefore, the temperature quickly decreases. In addition, expansion strongly stresses intermolecular bonds, ejecting small clusters and monomers along the wall surface and thus starting the fragmentation of the droplet into clusters. (iii) During 14–60 ps large voids appear in the droplet due to the tensile pressure forming now in the expanding fluid. The voids eventually tear the fluid to individual clusters; thus the maximum cluster size drops dramatically at the end of this void formation stage, while the temperature reaches equilibrium. (iv) After 60 ps, the dynamic droplet fragmentation process is over; cluster decomposition now continues mainly by monomer evaporation. In this evaporation stage, the size of the largest cluster does not change appreciably in our time scale.

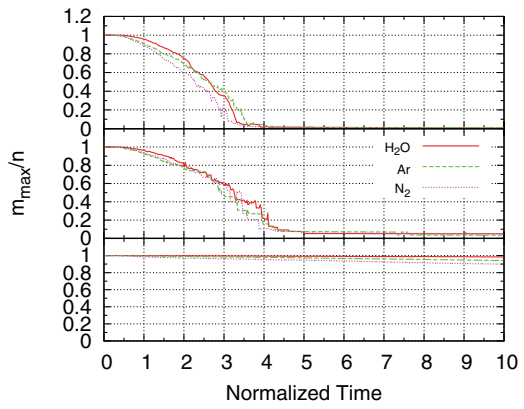

FIG. 3. (Color online) Comparison of the evolution of the size of the largest cluster m_{max} (normalized to the initial droplet size n) for Ar, N_2, and H_2O droplet-wall collisions. The scaled impact energies amount to $E/E_{coh} = 3.00$, 1.00, and 0.30 from top to bottom. Time t is scaled to the characteristic time τ [Eq. (1)] the droplet needs to fly through a distance equal to the droplet radius. The vertical line at normalized time $t/\tau = 4.3$ separates the fragmentation stage from the evaporation stage.

In the evaporation stage, the temperature of the largest droplet assumes values around 60–65 K; this is close to the melting point of N_2. Such low temperatures are commonly reached by evaporational cooling of small droplets, as has been shown, in particular, in studies of H_2O droplet evaporation [24–26]. Note that the rotational and translational temperatures are quite well equilibrated during the evaporation stage. During the fragmentation stage, however, rotation appears to be a few degrees hotter; this is due to the fact that droplet expansion and fragmentation primarily cool the translational degree of freedom.

We compare the dynamics of different droplets by normalizing time to the period of time needed to cover the droplet radius R with a velocity $\sqrt{2E/m}$:

$$\tau = \frac{R}{\sqrt{2E/m}}, \tag{1}$$

where m is the molecular mass. For the case of $E = E_{coh}$, it is $\tau = 14.44$, 13.87, and 4.22 ps for Ar, N_2, and H_2O, respectively.

Figure 3 demonstrates that after appropriate rescaling of time, the fragmentation dynamics of quite disparate materials becomes approximately similar, even though small differences remain. In particular, the fragmentation dynamics, shown for the scaled impact energies of $E/E_{coh} = 1.0$ and 3.0 in Fig. 3, satisfactorily coincide. This is possible even though the cluster constituents possess different numbers of internal degrees of freedom: the Ar atom possesses only translational degrees of freedom, while N_2 has two and H_2O has three rotational degrees of freedom. However, for bond breaking the total kinetic energy per molecule can be used, i.e., both rotational and translational energy can contribute; in this respect, atomic clusters and nonvibrating molecular clusters are expected to have similar fragmentation patterns, as evidenced in Fig. 3. Note that clusters composed of flexible molecules, in which vibrations can be excited, behave differently, as shown in Ref. [10]. However, for the excitation energies relevant for our study, vibrations cannot be excited in N_2 and H_2O. We hence learn from Fig. 3 that the droplet fragmentation process is governed by the ratio of the total available energy E per molecule and the cohesive energy E_{coh} needed to be overcome for bond breaking and hence for fragmentation. Figure 3 also shows a case of low-energy impact $E/E_{coh} = 0.3$; here the droplet does not fragment, but is only heated up and loses molecules by evaporation. In this case, the dynamics is not universal, but is governed by the evaporation rate determined by the temperature, to which the droplet has been heated by the collision, and by the heat of evaporation. We therefore do not expect this dynamics to be dictated by the single material parameter E_{coh}.

To describe the fragmentation process in a quantitative way, we introduce four measures: the number of fragments N_{fr}, the average fragment size $\langle m \rangle$, the size of the largest fragment

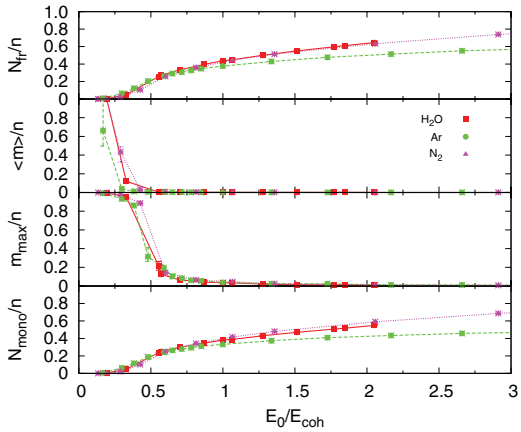

FIG. 4. (Color online) Dependence of fragmentation parameters (including error bars) on scaled energy E/E_{coh}.

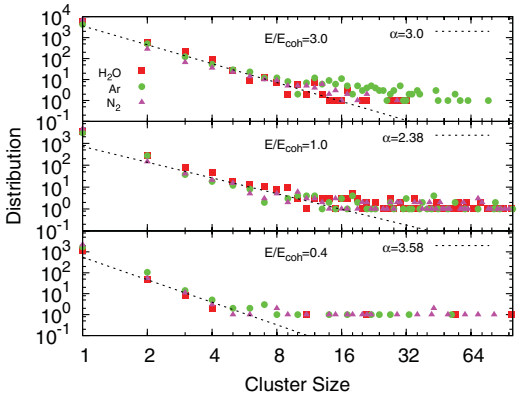

FIG. 5. (Color online) Distribution of fragment sizes for three normalized impact energies E/E_{coh}. The dashed line is a fit to the power-law distribution Eq. (2). The values of the exponent α are indicated.

m_{max}, and the number of free monomers created N_{mono}. Figure 4 shows the evolution of these quantities (measured at the end of the simulation time) with impact energy and Table I gathers the above-introduced fragmentation characteristics. It is observed that after scaling to the cohesive energy, the three materials studied behave in a remarkably similar way.

(i) The onset of the fragmentation regime is seen in the increase in the number of fragments and in the number of free monomers, in particular. Taking as an (arbitrary) threshold the energy when $N_{\mathrm{fr}}/n > 10\%$, fragmentation sets in at impact energies E/E_{coh} around 0.35–0.4 (Table I). At smaller impact energies, the tensile pressures produced in the lateral jetting phase are not strong enough to tear the droplet.

(ii) The onset of the fragmentation regime is accompanied by a sharp falloff of the average fragment size $\langle m \rangle$, which occurs at almost the same energies for the three different materials, $E/E_{\mathrm{coh}} \cong 0.29$–$0.40$ (Table I). These strong changes in the fragment distributions are reminiscent of a phase transition and have been characterized as such [7,27–31].

(iii) A regime of fully developed fragmentation might be tentatively characterized by requiring that no large fragment of the initial droplet survives; we have set $m_{\mathrm{max}}/n < 10\%$ as the limit. Fully developed fragmentation then starts at $E/E_{\mathrm{coh}} = 0.63$–$0.72$.

(iv) The fragmentation patterns of Ar deviate somewhat from those of the other two materials studied, in particular for high impact energies, where fragmentation produces fewer monomers N_{mono} and consequently fewer fragments N_{fr}. This is an indication that besides the major influence of the cohesive energy, other material parameters also influence (albeit in a minor way) details of the fragmentation process. A comparison between Ar and the equivalent (with respect to the thermophysical properties) N_2 can explain the difference: While Ar has an evaporation enthalpy of 67 meV, N_2 has only 30 meV, thus explaining the more efficient evaporation from N_2.

(v) While the complete disintegration of the droplet requires considerably higher impact energies, we observe that already more than 50% of the droplet has been fully disintegrated into its molecular constituents at $E/E_{\mathrm{coh}} = 1.7$–3.8.

In Fig. 5 we display the distributions of fragment size $f(m)$ for three impact energies $E/E_{\mathrm{coh}} = 0.4$, 1.0, and 3.0 for the three materials studied. In order to quantify these dependences, we fit their low-m behavior to a power-law distribution

$$f(m) \propto m^{-\alpha}. \tag{2}$$

We note that the monomers were not used in this fit since their contribution is determined by evaporation rather than by the fragmentation process. It is observed that the general features of the cluster distributions agree for the three materials. At the smallest impact energy $E/E_{\mathrm{coh}} = 0.4$, the distribution is steepest, while the slowest decay is observed for $E/E_{\mathrm{coh}} = 1.0$. For larger impact energies, the distribution steepens again. The reason for this dependence is intuitively clear: At small impact energies, droplet energization will lead mainly to smaller clusters plus a few large fragments, while at large impact energies, the energization is sufficient not only to tear the droplet into many pieces but also to destroy any larger fragments; in both cases, predominantly small clusters and a steep fragment distribution result. Hence, at intermediate energies, the maximum cluster abundance can be expected. We note that these features are in agreement with a recent study comparing the fragmentation distributions for H_2O and SO_2 clusters [32].

Theories of fragmentation usually predict exponential distributions $f(m) \propto m^{-\alpha} \exp(-bm^c)$. Such theories originate either by assuming fragmentation to occur in local thermodynamic equilibrium such that b depends on the local temperature achieved during fragmentation [33–35] or by interpreting fragmentation via percolation theory such that b depends on the percolation probability at the time of fragmentation [36]. Both these theories predict a pure power-law decay at their respective critical points, where cluster production at all sizes is most abundant: the thermodynamic model at the critical point of the liquid-gas phase transition where b vanishes and the power exponent a obeys $2 < \alpha < 2.5$ mildly dependent on the materials properties and the percolation model at the critical point of percolation $\alpha = 2.18$ [37]. We observe that the minimum exponent observed by us, $\alpha = 2.38$ at $E = E_{\mathrm{coh}}$, is in fair agreement with those of the two models just described at their respective critical points. We note that in a previous investigation of cluster formation during fragmentation of a solid under intense short-pulse laser

irradiation, it was observed that cluster formation is most abundant when $E \cong E_{\mathrm{coh}}$ [38] and can be described by a power-law distribution in the small-fragment regime [39]. In summary, our simulation results corroborate the finding of Ref. [32] that exponential distributions may be too steep to describe fragment size distributions in droplet-wall collisions.

IV. CONCLUSION

The essential message of Fig. 4 and Table I is that a single material property, the cohesive energy E_{coh}, describes the fragmentation patterns for different classes of materials rather well: atomic and molecular substances and van der Waals–bonded and polar-bonded materials. While it is plausible that the intermolecular bonding, which is quantified by the cohesive energy, is an important characteristics to describe fragmentation, it might be argued that the internal degrees of freedom of the molecular constituents also play an important role. In particular, the comparison of Ar and N_2, with similar thermophysical properties, shows that internal degrees of freedom play a minor role.

Furthermore, our simulations show that droplet disintegration does not require an energy of E_{coh} per molecule to start: It commences already at $(0.35–0.4)E_{\mathrm{coh}}$. When the impact energy reaches E_{coh}, droplet fragmentation is already fully developed in the sense described above: The number of isolated monomers has reached 33–42%, and the largest fragment contains only around 3.4–3.9% of the initial droplet size. Complete disintegration of the entire droplet will, however, take around 100 times higher impact energies.

ACKNOWLEDGMENTS

The authors acknowledge financial support from the Deutsche Forschungsgemeinschaft via the Graduiertenkolleg No. 792.

[1] W. Harbich, in *Metal Clusters at Surfaces: Structure, Quantum Properties, Physical Chemistry*, edited by K.-H. Meiwes-Broer, Springer Series in Cluster Physics (Springer, Berlin, 2000), p. 107.
[2] I. Yamada, J. Matsuo, Z. Insepov, T. Aoki, T. Seki, and N. Toyoda, Nucl. Instrum. Methods Phys. Res. Sect. B **164-165**, 944 (2000).
[3] W. Christen and U. Even, J. Phys. Chem. A **102**, 9420 (1998).
[4] S. A. Aksyonov and P. Williams, Rapid Commun. Mass Spectrom. **15**, 2001 (2001).
[5] S. N. Sun and H. M. Urbassek, J. Phys. Chem. B **115**, 13280 (2011).
[6] C. L. Cleveland and U. Landman, Science **257**, 355 (1992).
[7] T. Raz, U. Even, and R. D. Levine, J. Chem. Phys. **103**, 5394 (1995).
[8] W. Christen, U. Even, T. Raz, and R. D. Levine, Int. J. Mass Spectrom. Ion Processes **174**, 35 (1998).
[9] W. Christen, U. Even, T. Raz, and R. D. Levine, J. Chem. Phys. **108**, 10262 (1998).
[10] S. Zimmermann and H. M. Urbassek, Eur. Phys. J. D **39**, 423 (2006).
[11] S. Zimmermann and H. M. Urbassek, Phys. Rev. A **74**, 063203 (2006).
[12] A. Tomsic, H. Schröder, K.-L. Kompa, and C. R. Gebhardt, J. Chem. Phys. **119**, 6314 (2003).
[13] A. Tomsic, P. U. Andersson, N. Markovic, and J. B. C. Pettersson, J. Chem. Phys. **119**, 4916 (2003).
[14] J. Eggers, M. A. Fontelos, C. Josserand, and S. Zaleski, Phys. Fluids **22**, 062101 (2010).
[15] A. L. Yarin, Annu. Rev. Fluid Mech. **38**, 159 (2006).
[16] R. A. Aziz, J. Chem. Phys. **99**, 4518 (1993).
[17] T. A. Scott, Phys. Rep. **27**, 69 (1976).
[18] C. S. Murthy, K. Singer, M. L. Klein, and I. R. McDonald, Mol. Phys. **41**, 1387 (1980).
[19] W. L. Jorgensen, J. Chandrasekhar, J. D. Madura, R. W. Impey, and M. L. Klein, J. Chem. Phys. **79**, 926 (1983).
[20] R. E. Johnson, *Energetic Charged-Particle Interactions with Atmospheres and Surfaces* (Springer, Berlin, 1990).
[21] H. Gades and H. M. Urbassek, Phys. Rev. B **51**, 14559 (1995).
[22] K. K. Haller, Y. Ventikos, D. Poulikakosa, and P. Monkewitz, J. Appl. Phys. **92**, 2821 (2002).
[23] M. Rein, Fluid Dyn. Res. **12**, 61 (1993).
[24] C. Caleman and D. van der Spoel, J. Chem. Phys. **125**, 154508 (2006).
[25] E. G. Marklund, D. S. D. Larsson, D. van der Spoel, A. Patriksson, and C. Caleman, Phys. Chem. Chem. Phys. **11**, 8069 (2009).
[26] S. P. Thirumuruganandham and H. M. Urbassek, Biochem. Res. Int. **2010**, 213936 (2010).
[27] O. Sotolongo-Costa, Y. Moreno-Vega, J. J. Lloveras-González, and J. C. Antoranz, Phys. Rev. Lett. **76**, 42 (1996).
[28] A. Strachan and C. O. Dorso, Phys. Rev. C **55**, 775 (1997).
[29] A. Strachan and C. O. Dorso, Phys. Rev. C **58**, R632 (1998).
[30] F. Kun and H. J. Herrmann, Phys. Rev. E **59**, 2623 (1999).
[31] H. Katsuragi, D. Sugino, and H. Honjo, Phys. Rev. E **68**, 046105 (2003).
[32] A. Tomsic and C. R. Gebhardt, J. Chem. Phys. **123**, 064704 (2005).
[33] M. E. Fisher, Physics **3**, 255 (1967).
[34] M. E. Fisher, Rep. Prog. Phys. **30**, 615 (1967).
[35] H. M. Urbassek, Nucl. Instrum. Methods Phys. Res. Sect. B **31**, 541 (1988).
[36] A. L. Yarin, *Free Liquid Jets and Films: Hydrodynamics and Rheology* (Wiley, New York, 1993).
[37] D. Stauffer and A. Aharony, *Introduction to Percolation Theory*, 2nd ed. (Taylor and Francis, London, 1994).
[38] T. J. Colla and H. M. Urbassek, Comput. Mater. Sci. **6**, 7 (1996).
[39] A. K. Upadhyay and H. M. Urbassek, Phys. Rev. B **73**, 035421 (2006).